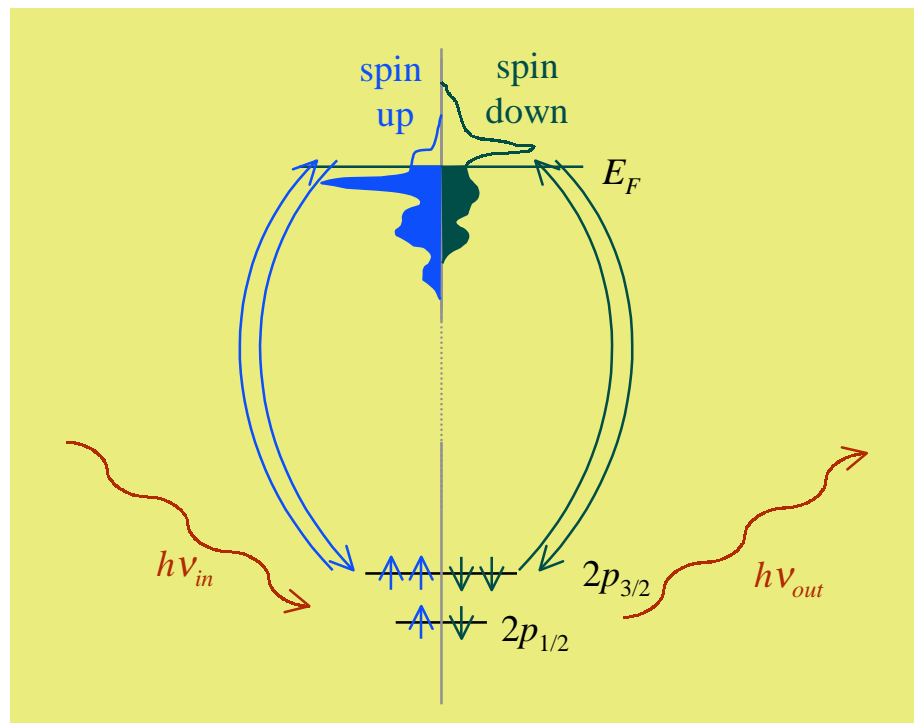
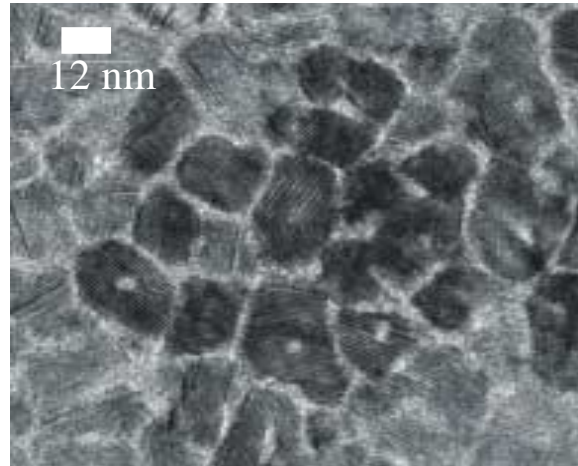
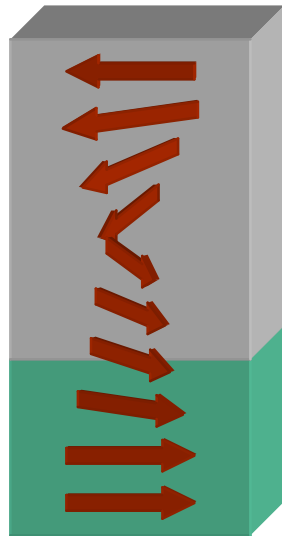


Resonant x-ray magneto-optical spectroscopies - beyond MCD



J. B. Kortright
MSD, LBNL

E. E. Fullerton, O. Hellwig, K. Takano,
D. T. Marguiles, G. Zeltzer
IBM Almaden Research Center
J. S. Jiang, and S. D. Bader
Argonne National Laboratory

Sang-Koog Kim
Seoul National U., South Korea
S. D. Kevan
U. Oregon
L. Sorenson
U. Washington

Overview.

Motivation

Theory of resonant magneto-optical (MO) effects:

- atomic scattering factor (microscopic)
- dielectric tensor (macroscopic)

Applications:

- MO Kerr & Faraday effects, “scattering”
- Specific examples:
 - Faraday rotation: Fe MO constants
 - XMOKE: exchange-spring magnets
 - Diffuse scattering (Co/Pt multilayers, recording media)

Motivation.

Soft x-ray region contains core-levels of magnetic elements:

- 3d transition elements
- 4f rare earths

Extend photon-based (quasi-elastic scattering) techniques to these core levels:

- MO Kerr and Faraday effects (from visible)
- scattering/diffraction techniques (hard x-ray, visible)
- microscopy techniques (from visible)

Need to understand and apply relevant spectroscopic theories to plan experiments and analyze data.

Large resonant enhanced scattering at soft x-ray core levels.

2p levels couple to spin polarized
3d states via *dipole* transitions.

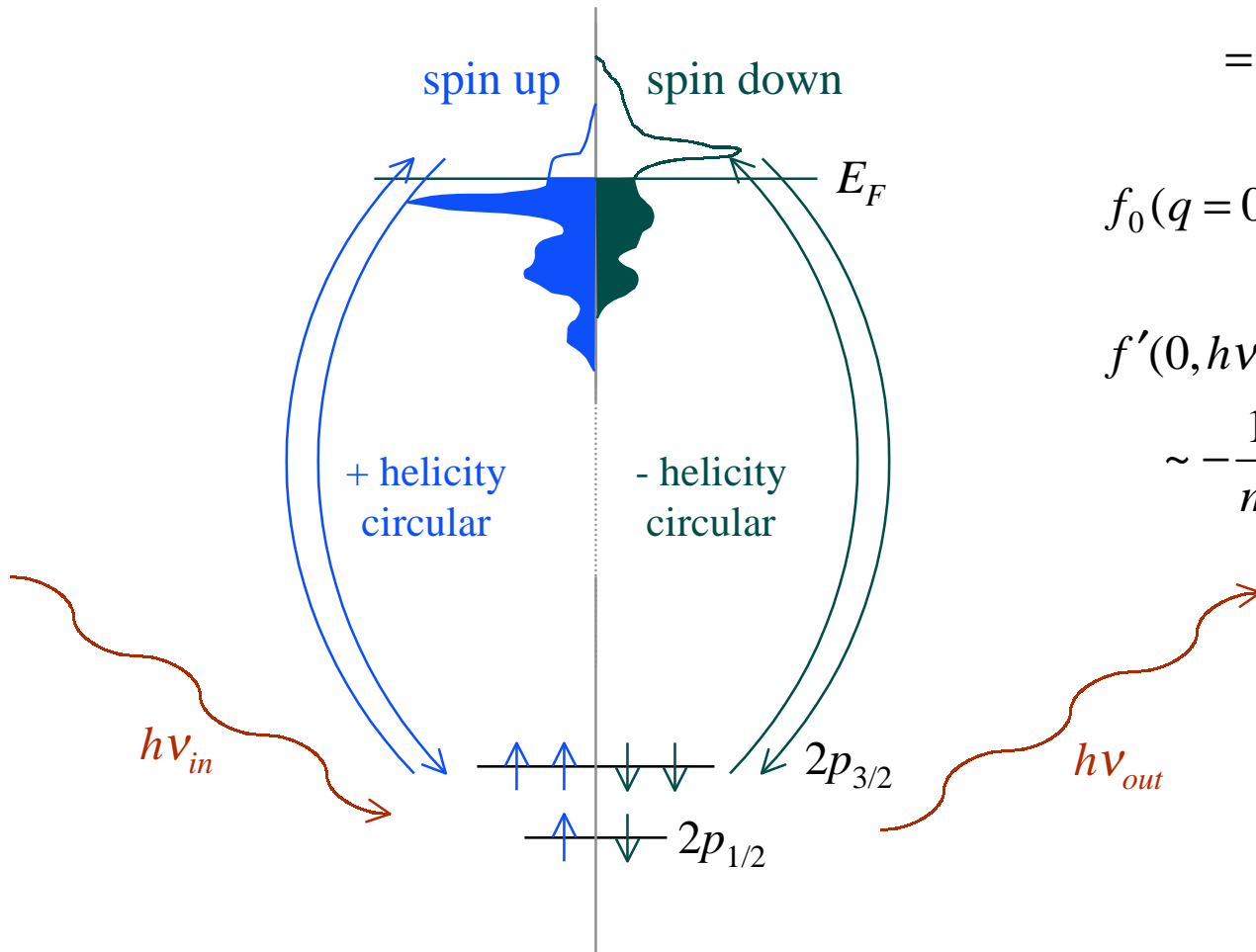
$$f(q, h\nu) = f_0(q) + f'(q, h\nu) + if''(q, h\nu)$$

$$= f_1(q, h\nu) + if_2(q, h\nu)$$

$$f_0(q=0) \sim Z$$

$$f'(0, h\nu) + if''(0, h\nu)$$

$$\sim -\frac{1}{m} \sum_n \frac{\langle b | \mathbf{p} \cdot \mathbf{A} | n \rangle \langle n | \mathbf{p} \cdot \mathbf{A} | a \rangle}{E_a - E_n + i\Gamma}$$



Linear polarization = (+) + (-) helicities

The resonant atomic scattering factor.

Hannon, Trammel, Blume, Gibbs, PRL **61**, 1245, (1989)

Assume:

- electric dipole transitions only
- ignore non-resonant magnetic term

$$f = (\mathbf{e}_f^* \cdot \mathbf{e}_\theta) \left\{ \frac{3}{8\pi} \lambda [F_1^1 + F_{-1}^1] - r_e Z \right\} + \frac{3}{8\pi} \lambda \left\{ i(\mathbf{e}_f^* \times \mathbf{e}_\theta) \cdot \mathbf{m} [F_{-1}^1 - F_1^1] + (\mathbf{e}_f^* \cdot \mathbf{m})(\mathbf{e}_\theta \cdot \mathbf{m}) [2F_0^1 - F_1^1 - F_{-1}^1] \right\}$$

1st order magnetic scattering, $\mathbf{k} \cdot \mathbf{M}$

$\mathbf{e}_{o,f}$ are unit polarization vectors of incident, scattered radiation

\mathbf{m} is local unit magnetization vector

F_M^L are dipole matrix elements resolved into different spherical harmonics $Y_{LM}(\theta, \phi)$

$$f = (\mathbf{e}_f^* \cdot \mathbf{e}_\theta) f_c + i(\mathbf{e}_f^* \times \mathbf{e}_\theta) \cdot \mathbf{m} f_{ml} + (\mathbf{e}_f^* \cdot \mathbf{m})(\mathbf{e}_\theta \cdot \mathbf{m}) f_{m2}$$

$$n(\omega) = 1 - \sum_i N_i r_e \lambda^2 f_i(\omega, 0) / 2\pi = 1 - \delta(\omega) + i\beta(\omega)$$

Visible MO description, equivalence with atomic scattering factor.

See, e.g., Frieser, IEEE Trans. Magn. **4**, 152 (1968)
Kortright & Kim, PRB **62**, 12216 (2000)

“Bulk” description uses dielectric tensor.
Assume cubic symmetry, \mathbf{M} along z.

$$\boldsymbol{\epsilon}(\omega) = \begin{pmatrix} \epsilon_{xx} & \epsilon_{xy} & 0 \\ -\epsilon_{xy} & \epsilon_{xx} & 0 \\ 0 & 0 & \epsilon_{zz} \end{pmatrix}.$$

$$n(\omega) \equiv \sqrt{\epsilon(\omega)} = 1 - \delta(\omega) + i\beta(\omega)$$

3 “normal modes” describe propagation of pure polarization states:

$$\mathbf{k} \parallel \mathbf{M} \quad n_{+/-} = \sqrt{\epsilon_{xx} \pm i\epsilon_{xy}} = 1 + Nr_e \lambda^2 (4\pi r_e Z - 3\lambda F_{-1/1}^1) / 8\pi^2$$

$$\mathbf{k} \perp \mathbf{M} \quad \mathbf{E} \parallel \mathbf{M} \quad n_{\parallel} = \sqrt{\epsilon_{zz}} = 1 - Nr_e \lambda^2 (4\pi r_e Z + 3\lambda F_0^1) / 8\pi^2$$

$$\mathbf{k} \perp \mathbf{M} \quad \mathbf{E} \perp \mathbf{M} \quad n_{\perp} = \sqrt{(\epsilon_{xx}^2 + \epsilon_{xy}^2) / \epsilon_{xx}} = 1 - Nr_e \lambda^2 (8\pi r_e Z + 3\lambda [F_1^1 + F_{-1}^1]) / 16\pi^2$$

Magnetic dichroism and birefringence.

Magnetic *circular* dichroism & birefringence (1st order):

$$n_+ - n_- = 3Nr_e\lambda^3[F_1^1 - F_{-1}^1]/8\pi^2 \propto 2f_{m1}$$

Magnetic *linear* dichroism & birefringence (2nd order):

$$n_\perp - n_\parallel = 3Nr_e\lambda^3[2F_0^1 - (F_1^1 + F_{-1}^1)]/16\pi^2 \propto f_{m2}$$

Many ways to measure these quantities.

Real and imaginary parts related by
Kramers-Kronig transformation.

Faraday rotation spectra for Fe yields 1st order MO constants.

$$\phi(\lambda) = [n_+(\lambda) - n_-(\lambda)]\pi t / \lambda$$

$$n = 1 - \delta + i\beta$$

Phase contrast from $\text{Re}[\phi(\lambda)]$

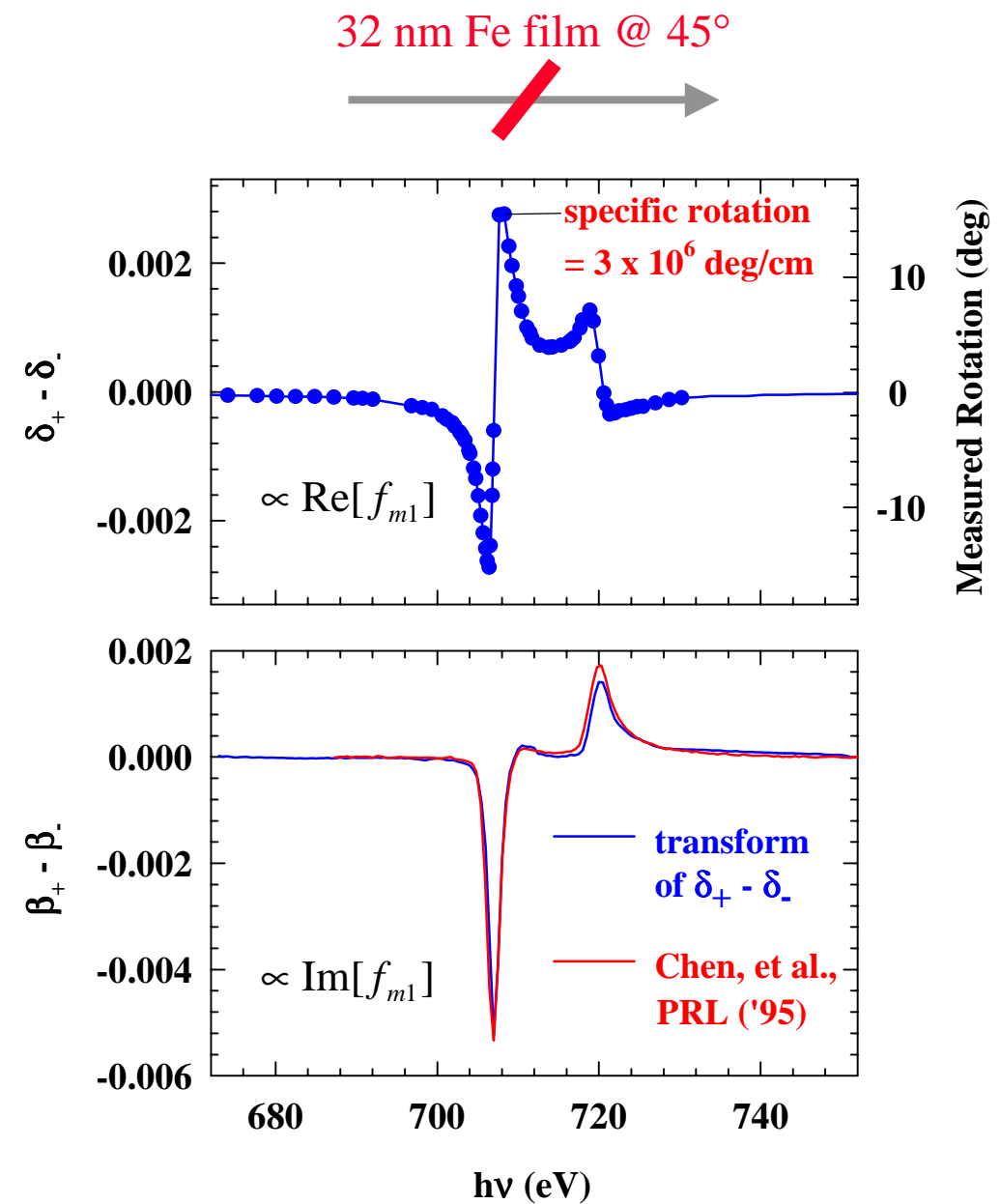
Faraday rotation, *linear* polarization.

$(\delta_+ - \delta_-)\pi t / \lambda = 15^\circ$ at resonance!

Linear polarizer analyzes phase.

Amplitude contrast from $\text{Im}[\phi(\lambda)]$

MCD using *circular* polarization.

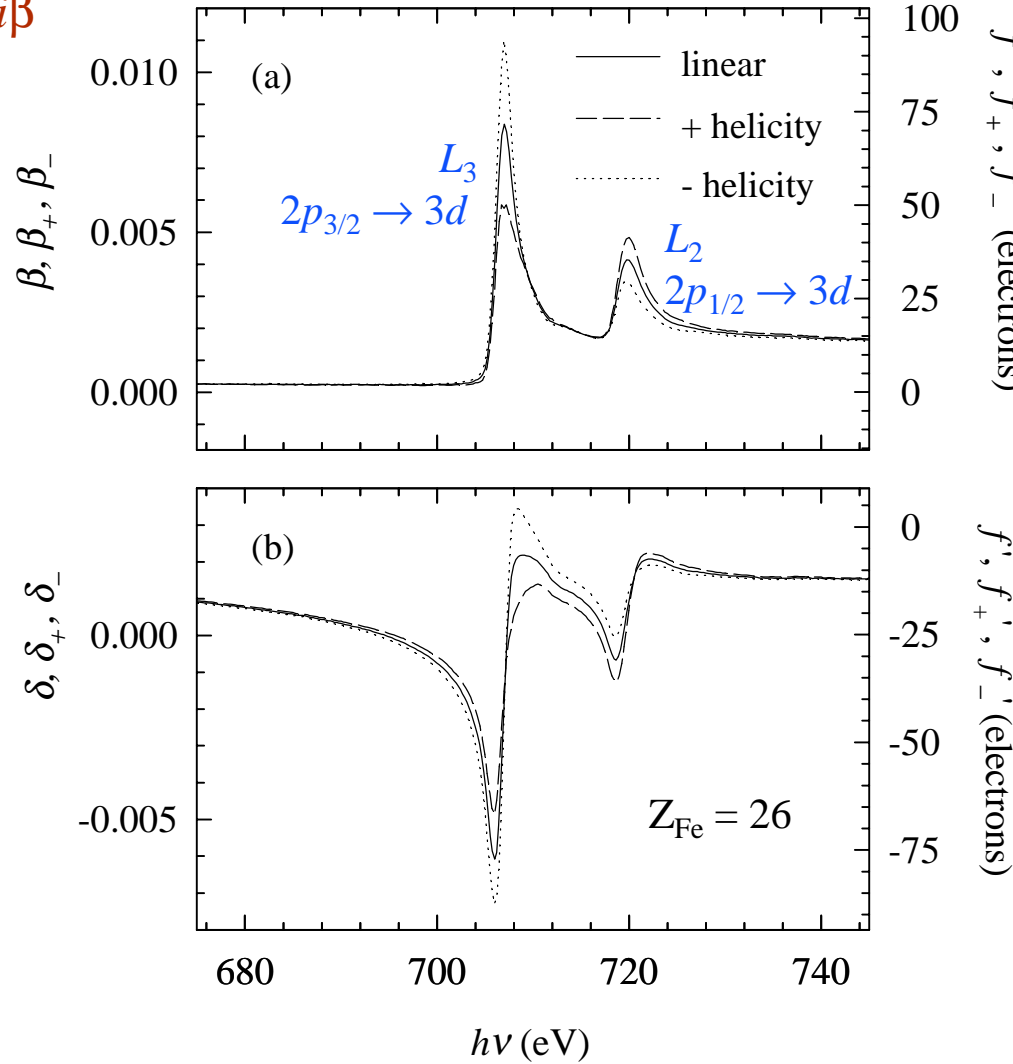


1st order MO constants for Fe.

Kortright & Kim, PRB **62**, 12216 (2000)

“Bulk” description:

$$n = 1 - \delta + i\beta$$



“Atomic” description:

$$f = f_o + f' + if''$$

$$f_{lin} = (f_+ + f_-)/2 = f_c$$

$$f_+ = f_c + f_{m1}$$

$$f_- = f_c - f_{m1}$$

2nd order MO effect (Voigt effect) is small for bulk bcc Fe.

Kortright & Kim, PRB 62, 12216 (2000)

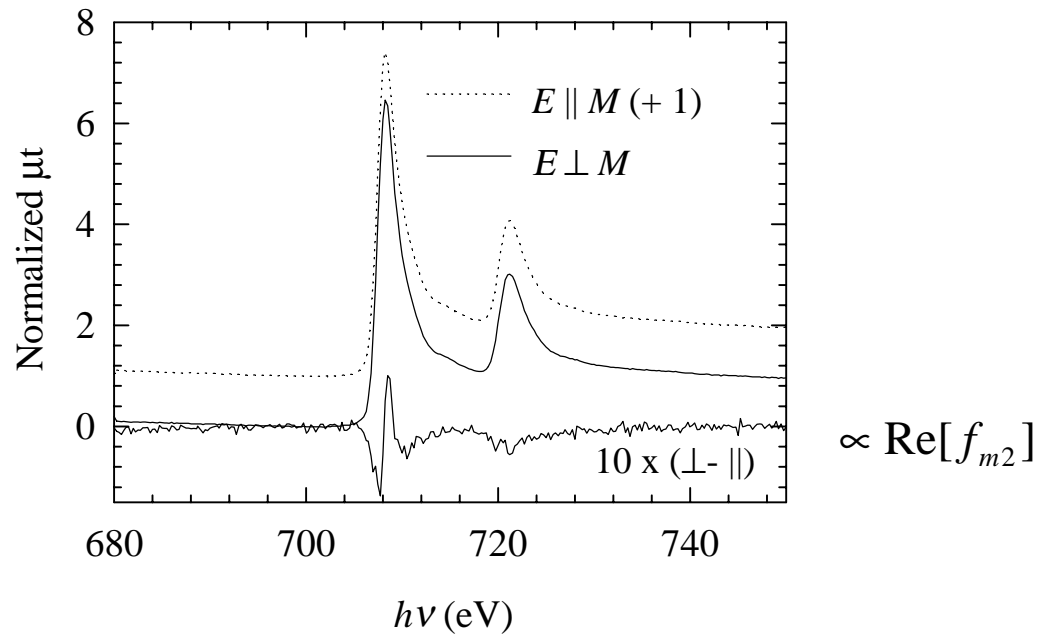


Figure 5

Measurable MO quantities include polarization *and* intensity changes on change of sample magnetization.

Faraday MO effects in transmission

1st order, complex Faraday rotation:

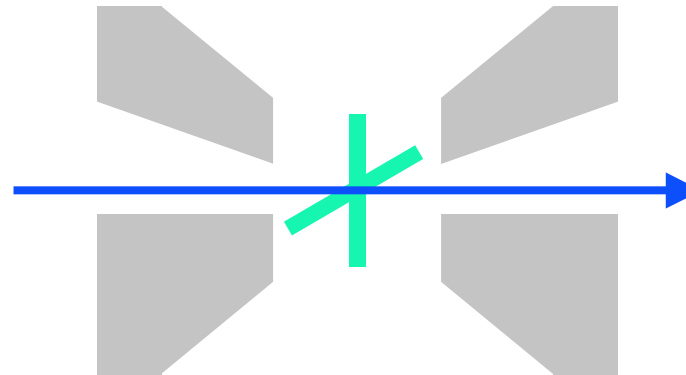
$$\phi_F = (n_+ - n_-)\pi t / \lambda = \alpha_F - i\epsilon_F$$

$$\alpha_F = \delta_+ - \delta_- \text{ is MCB}$$

$$\epsilon_F = \beta_+ - \beta_- \text{ is MCD}$$

2nd order, Voigt effect:

$$n_{\perp} - n_{\parallel}, \text{MLD, MLB}$$



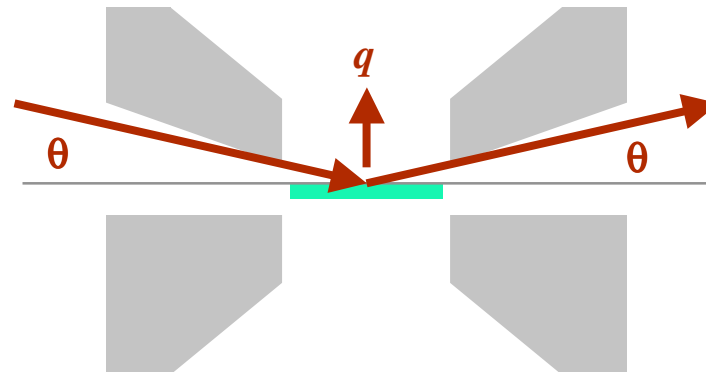
Kerr MO effects in reflection

Neglect 2nd order effects:

$$\boldsymbol{\epsilon} = n_0^2 \begin{pmatrix} 1 & iQ & 0 \\ -iQ & 1 & 0 \\ 0 & 0 & 1 \end{pmatrix}$$

$$\begin{pmatrix} \mathbf{E}_s^R \\ \mathbf{E}_p^R \end{pmatrix} = \begin{pmatrix} r_{ss} & r_{sp} \\ r_{ps} & r_{pp} \end{pmatrix} \begin{pmatrix} \mathbf{E}_s^o \\ \mathbf{E}_p^o \end{pmatrix}$$

$$\phi_{K,s} = r_{ps}/r_{ss} = \alpha_K + i\epsilon_K$$

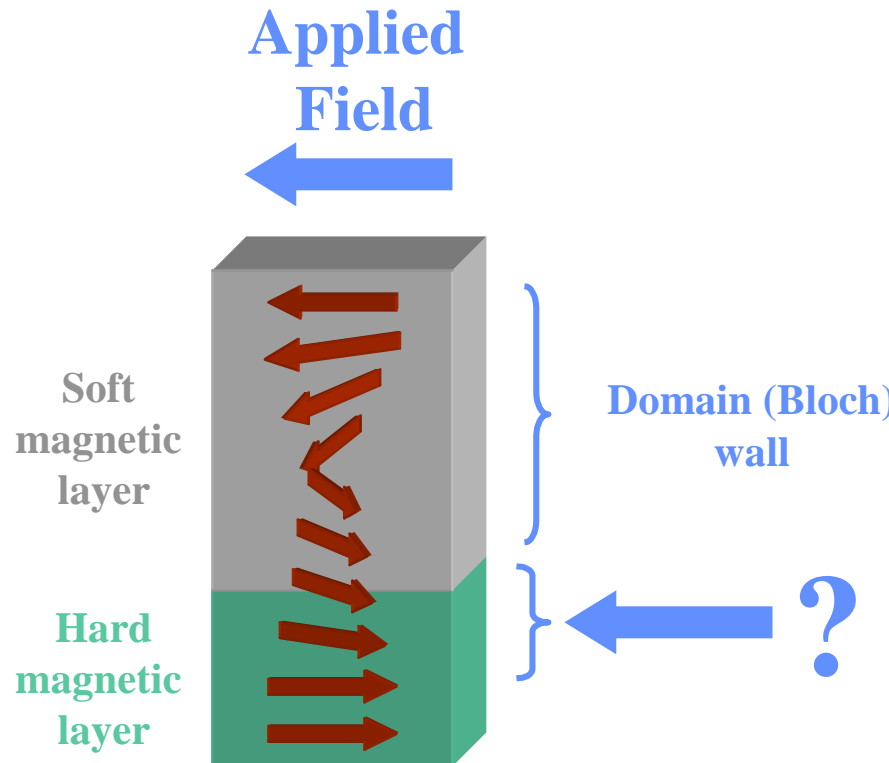


Need resonant MO constants n_+ , n_- , or n_0 , Q for quantitative modeling, planning.

1. XMOKE studies of exchange-spring heterostructures.

Hellwig, et al, PRB 62, 11694 (00)
Kortright, et al., NIM A 467, 1396 (01)

Use exchange hardening to produce higher energy product hard magnets.



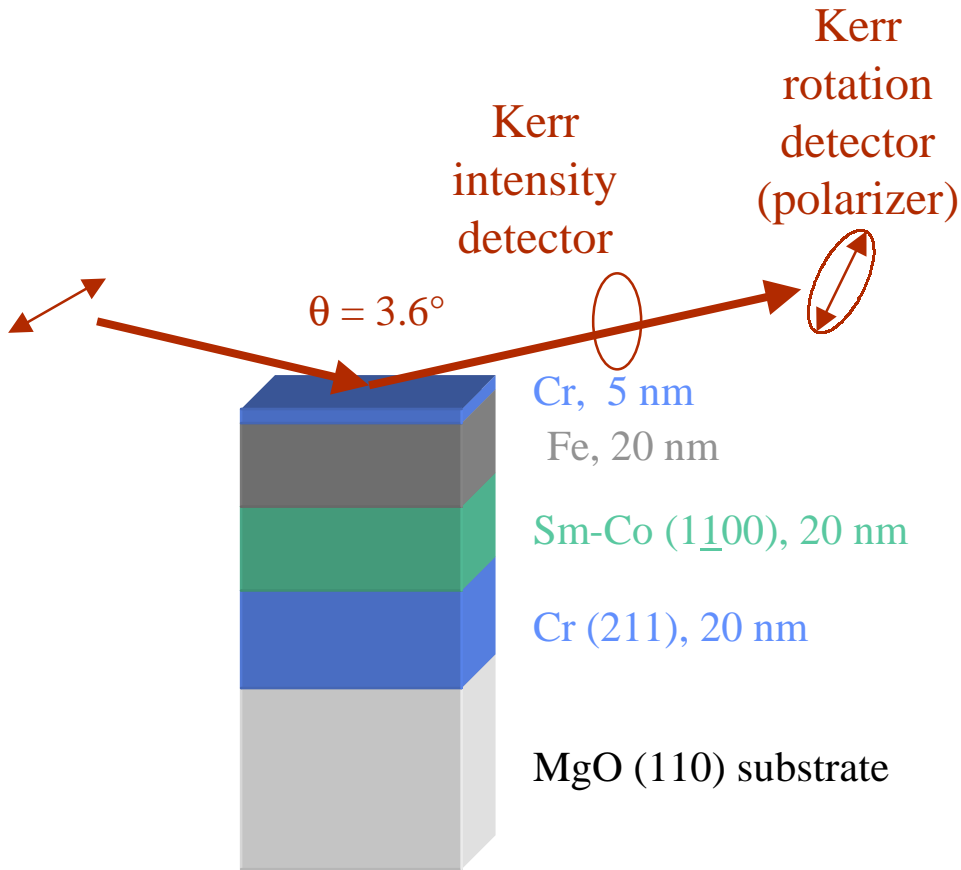
Simplest picture:
Soft layer forms twist in M in depth
that is entirely reversible until the hard
layer switches.

Question:
Is hard layer rigidly fixed until it reverses?

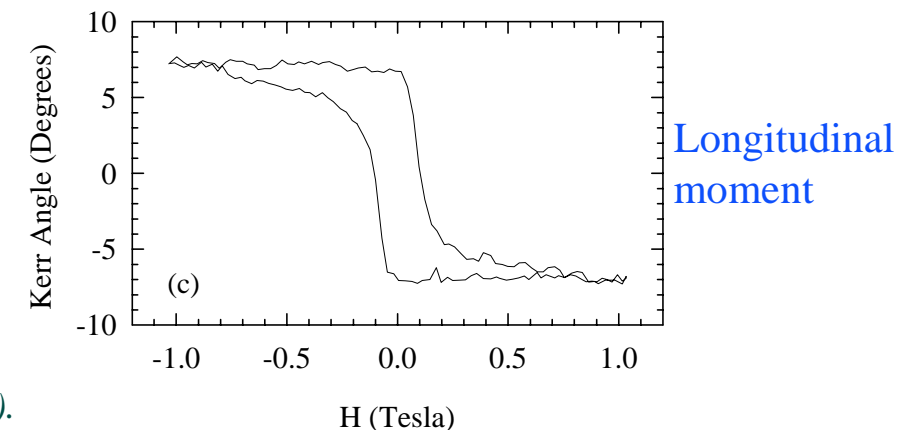
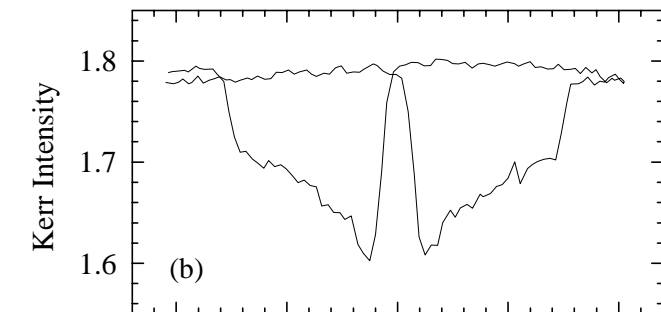
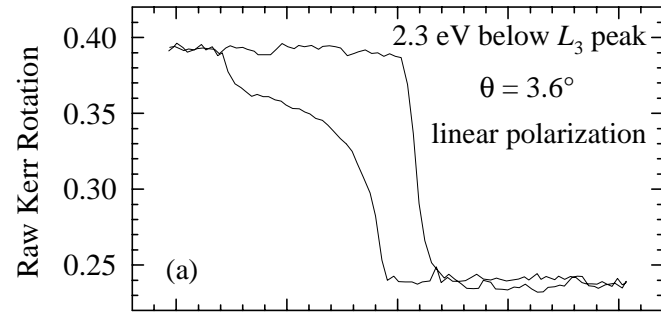
Two systems studied:

- Sm-Co/Fe (~ epitaxial, uniaxial)
- Fe-Pt/Ni-Fe (polycrystalline, textured)

Fe XMOKE resolves M spiral in Fe layer.



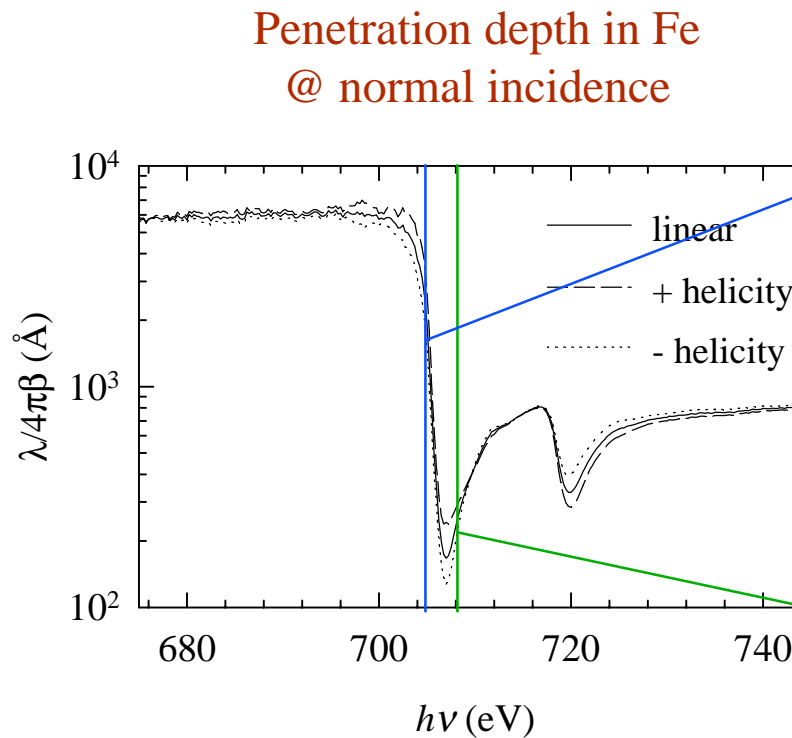
Linear (s) polarization @ Fe edge



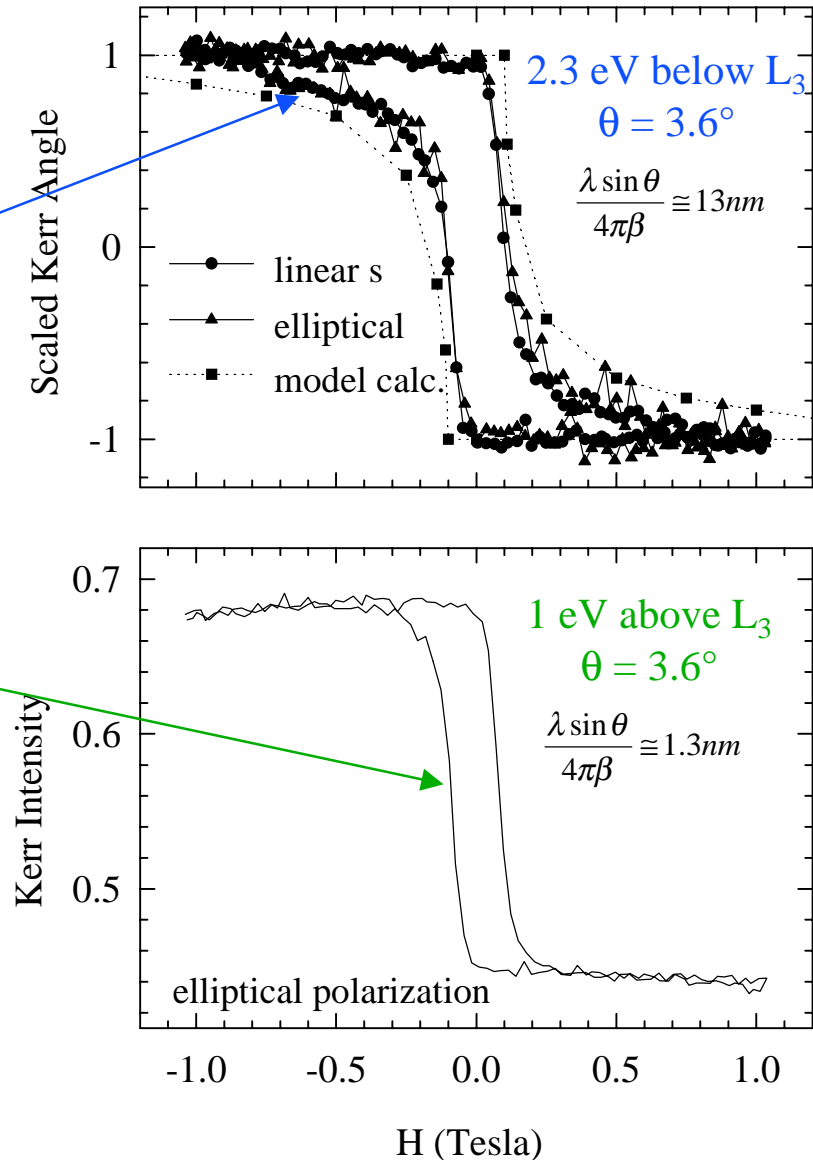
Kortright, Kim, Fullerton, Jiang, Bader, NIM A 467, 1396 (2001).

Variable depth sensitivity obtained by tuning to different energies near Fe L_3 line.

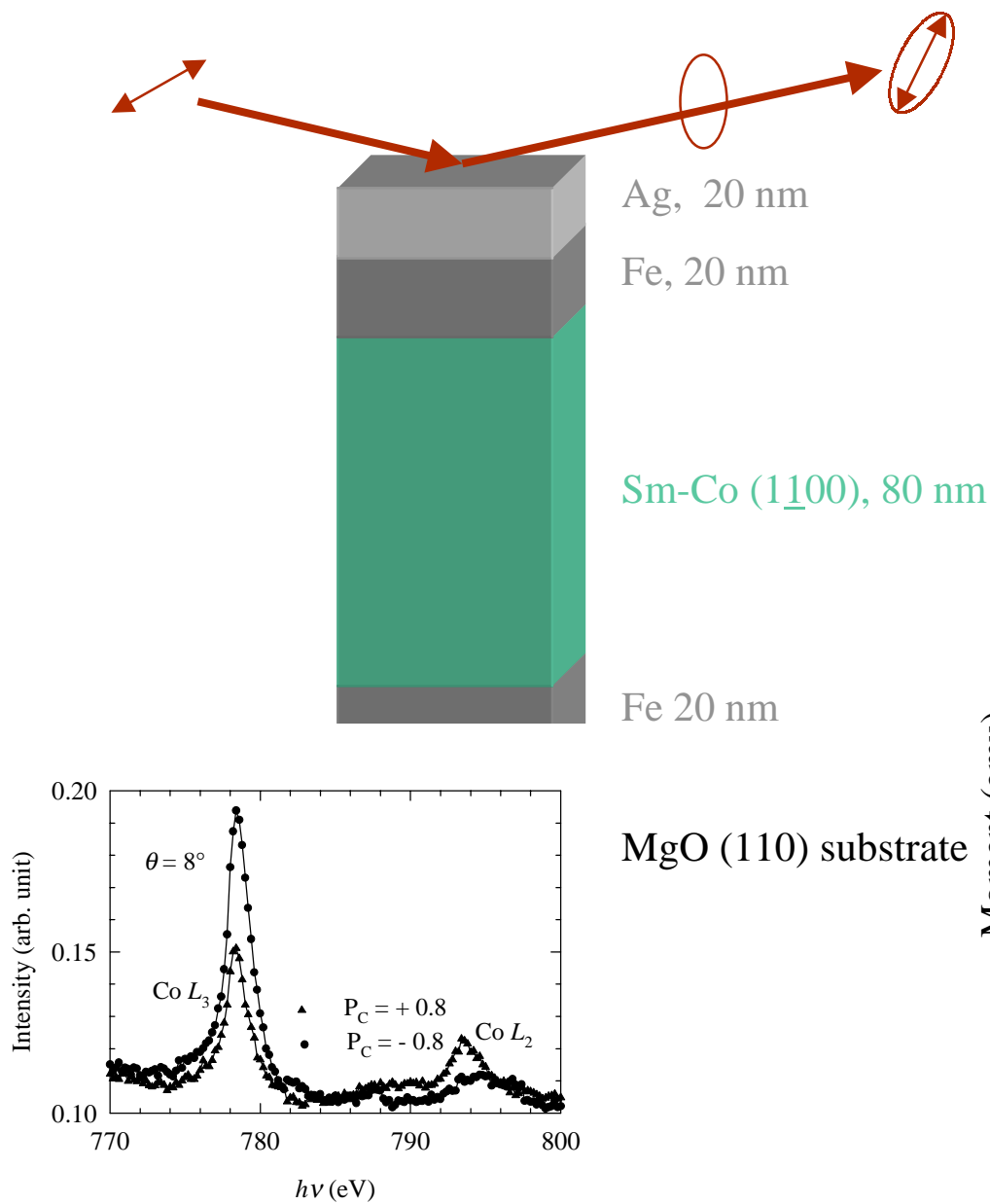
Kortright, Kim, Fullerton, Jiang, Bader, NIM A **467**, 1396 (2001)



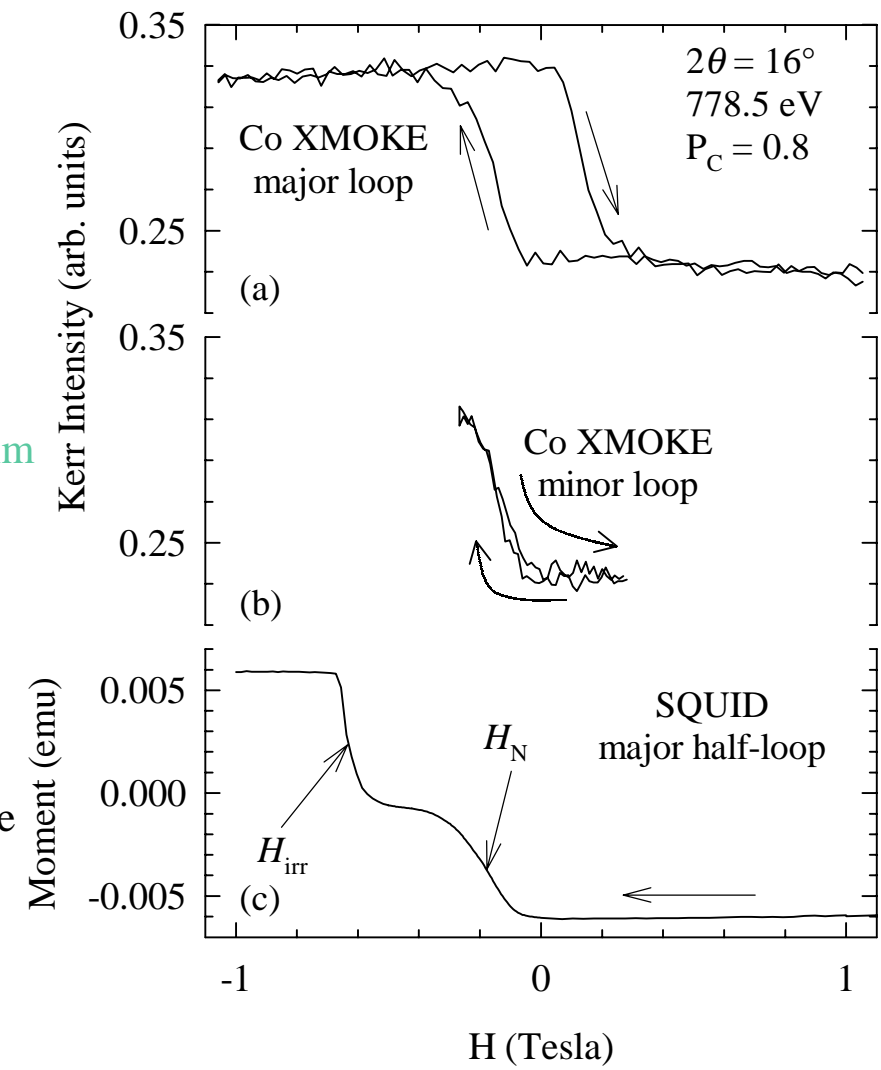
Direct, model-independent sensitivity
to reversal at different depths in Fe layer.



XMOKE from Co in Sm-Co layer confirms that part of it rotates reversibly with soft layer.

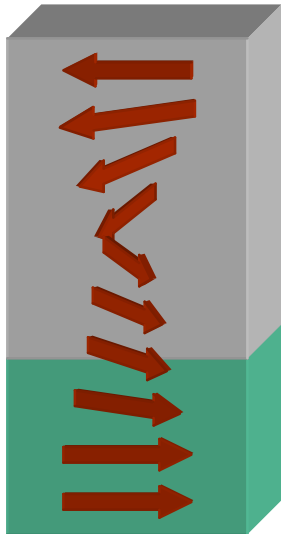


Kortright, Jiang, & Bader (submitted)



Top of Sm-Co layer shows reversible minor loop behavior.

Summary of exchange-spring studies.



Variable depth sensitivity through:

- chemical marker layers
- tuning to soft, hard core levels
- energy tuning across white line
- modeling longitudinal, transverse signals.

Considerably greater penetration depth than visible MO effects.

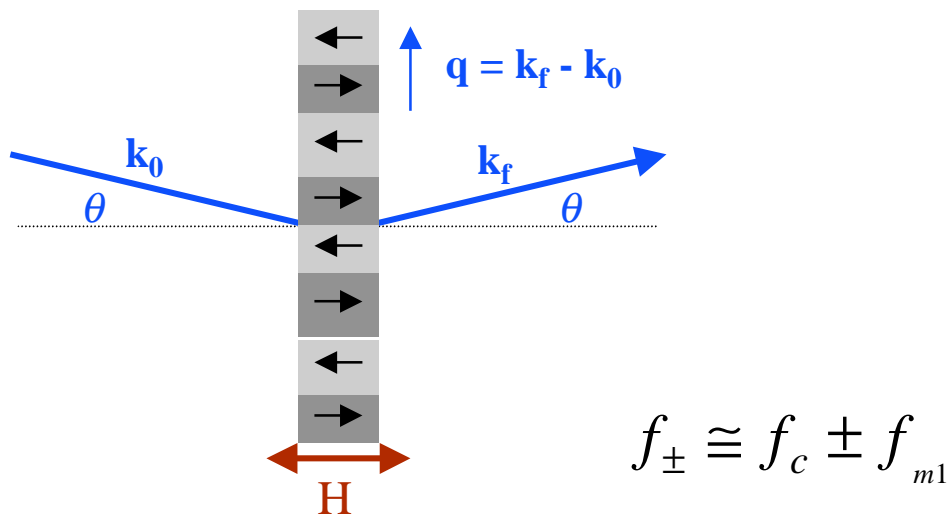
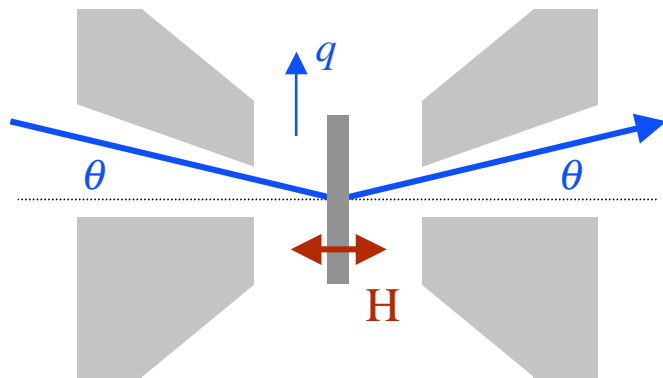
Confirmed coherent, reversible twist structure in soft layer.

Top of hard layer not rigidly pinned, but shows low-field, reversible motion \Rightarrow reversible energy stored not only in soft but also in hard layer.

2. Co/Pt multilayers: model systems to explore resonant magnetic scattering from magnetic *domains*.

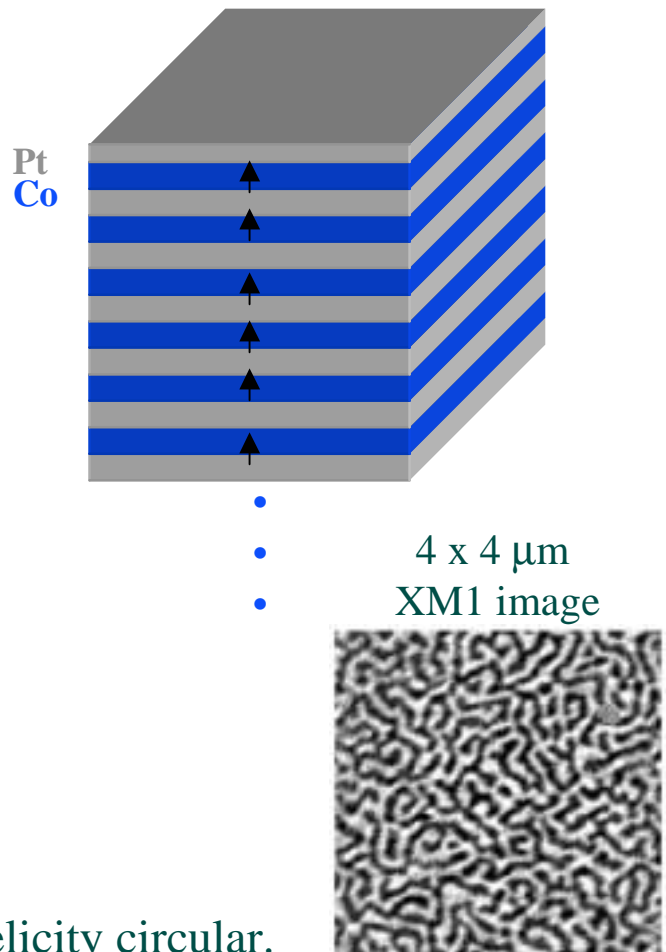
PRB 64, 092401 (01)

Traditional SAS geometry



Use *linear* polarization $\equiv (+) + (-)$ helicity circular.

Co/Pt multilayer films have
perpendicular anisotropy
for $t_{Co} < \sim 1$ nm



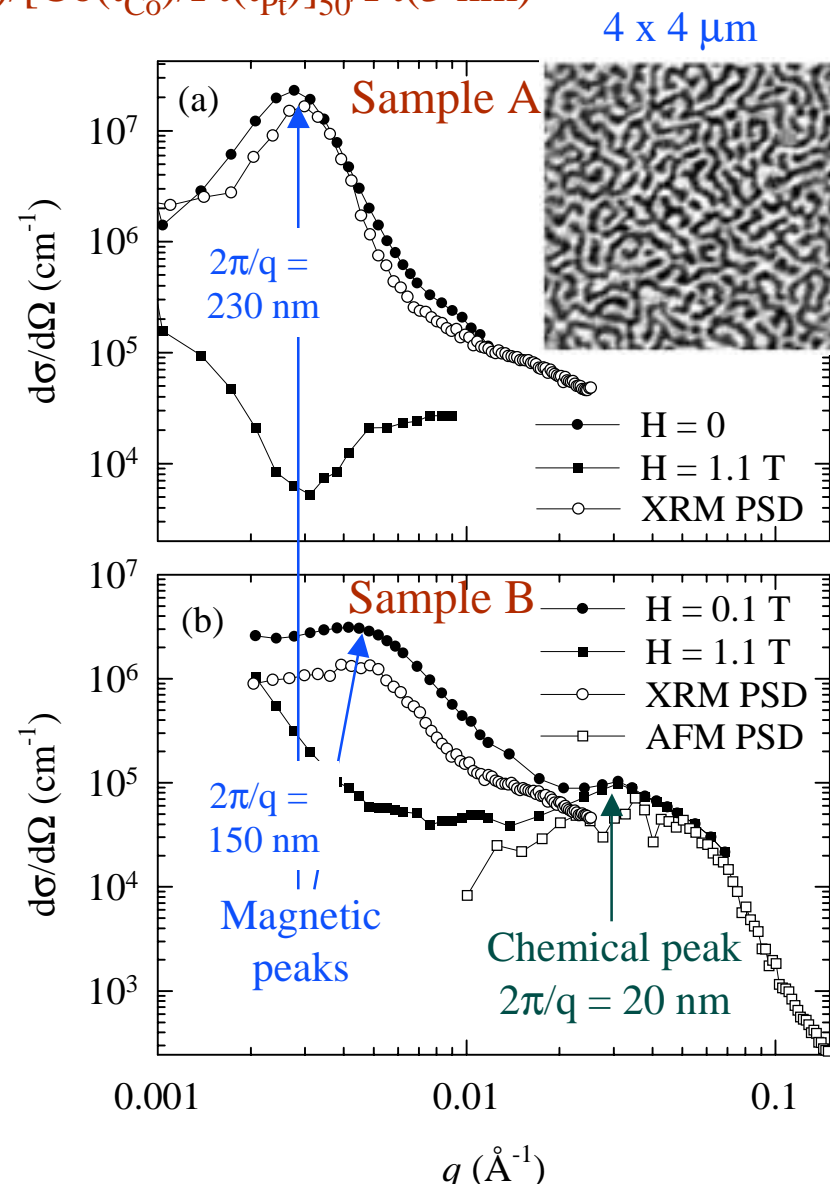
SAS q scans reveal two distinct length scales: magnetic domains and polycrystalline grains.

$\text{SiN}_x(160 \text{ nm})/\text{Pt}(20 \text{ nm})/[\text{Co}(t_{\text{Co}})/\text{Pt}(t_{\text{Pt}})]_{50}/\text{Pt}(3 \text{ nm})$

Samples designed to have low remnance
(high domain density)

Sample A: $T = 250^\circ \text{ C}$
 $t_{\text{Co}} = 0.4 \text{ nm}$
 $t_{\text{Pt}} = 0.7 \text{ nm}$

Sample B: $T = \text{RT}$
 $t_{\text{Co}} = 0.6 \text{ nm}$
 $t_{\text{Pt}} = 0.4 \text{ nm}$

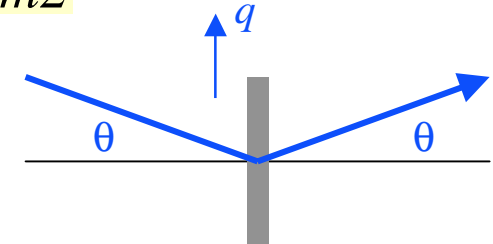


Theoretical considerations of magnetic, charge scattering.

PRB 64, 092401 (01)

$$f = (\mathbf{e}_f^* \cdot \mathbf{e}_o) f_c + i(\mathbf{e}_f^* \times \mathbf{e}_o) \cdot \mathbf{m} f_{m1} + (\mathbf{e}_f^* \cdot \mathbf{m})(\mathbf{e}_o \cdot \mathbf{m}) f_{m2}$$

Small θ , M perpendicular: $f_{\pm} \cong f_c \pm f_{m1}$



Contrast mechanism defines SAS amplitude: $a \propto a_A - a_B$, $a_A = \sum x_i f_i$

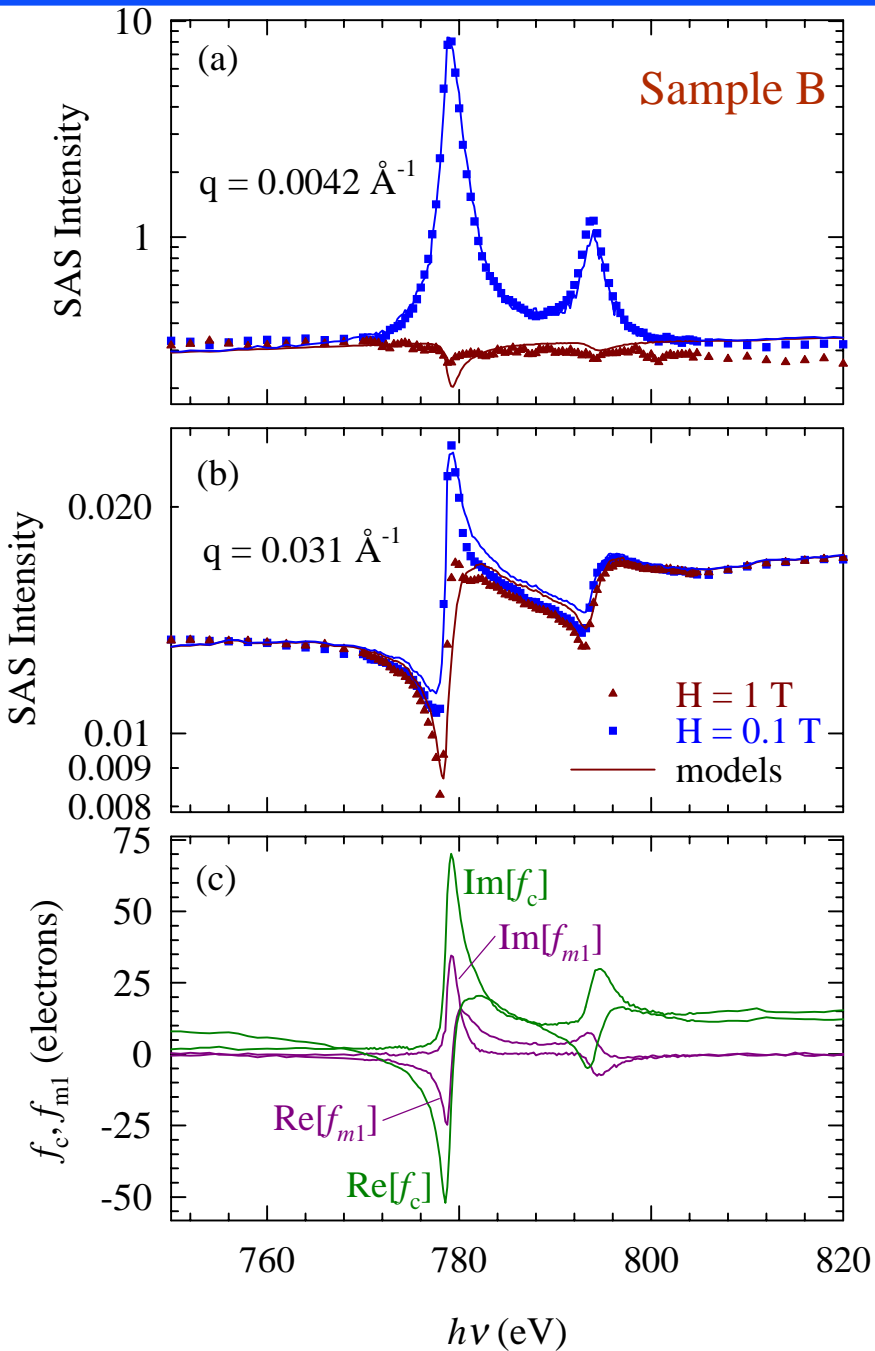
General amplitude for multiple scattering sources: $A = \sum_i a_i s_i$

Intensity assuming distinct magnetic and charge amplitudes:

$$A^* A = a_m^* a_m s_{m-m} + a_c^* a_c s_{c-c} + 2 \operatorname{Re}[a_m^* a_c] s_{m-c}$$

$$I \propto (A^* A) T$$

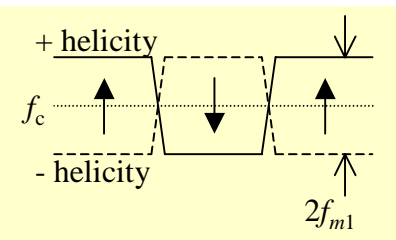
Spectral scans reveal magnetic, chemical contributions .



At magnetic peak

Pure magnetic

$$a = 2f_m$$



plus small chemical background

At charge peak

Pure chemical @ saturation

$$a = (f_{\text{Co},c} + 3f_{\text{Pt}}) - 0$$

Chemical + magnetic @ 0.1 T

Measured Co scattering factors

$$f_{+/-} = f_c +/- f_m$$

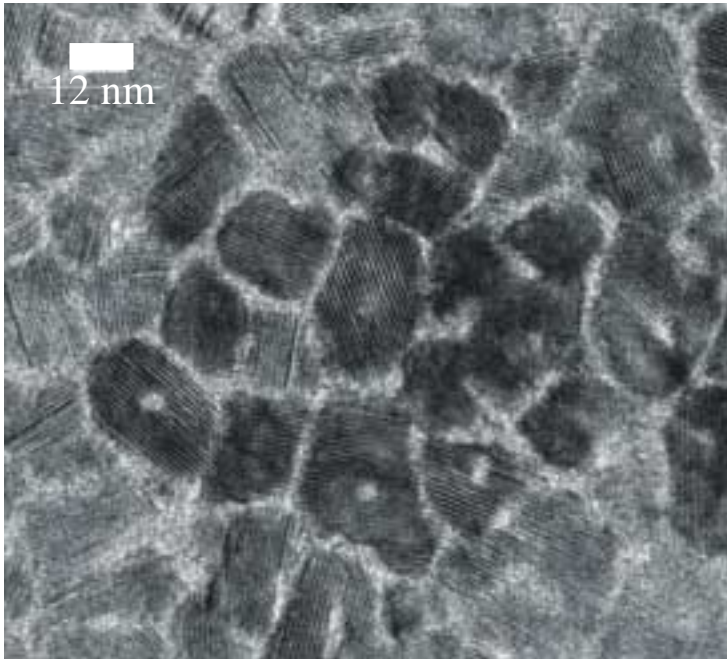
3. Longitudinal recording media: simultaneous characterization of magnetic & chemical length scales.

Adding B improves SNR, recording density.

How?

- Finer grain size?
- Narrows grain size distribution?
- Promotes segregation?
- Reduce intergrain exchange?

CoPtCrB



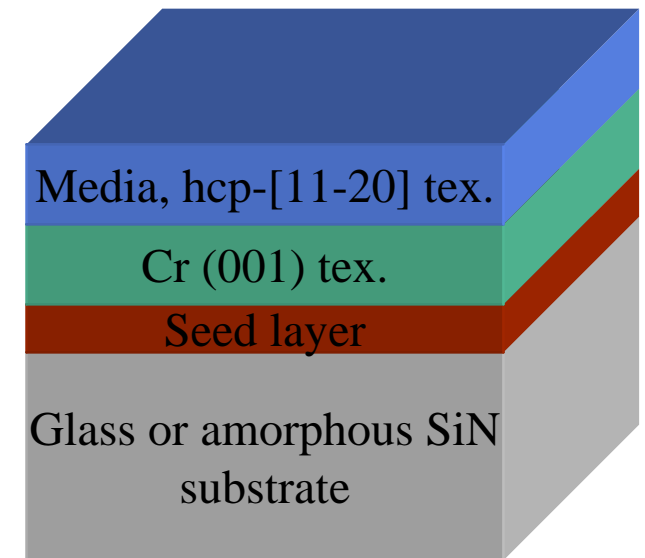
Magnetic correlation length ?

(image by Kai Tang, IBM)

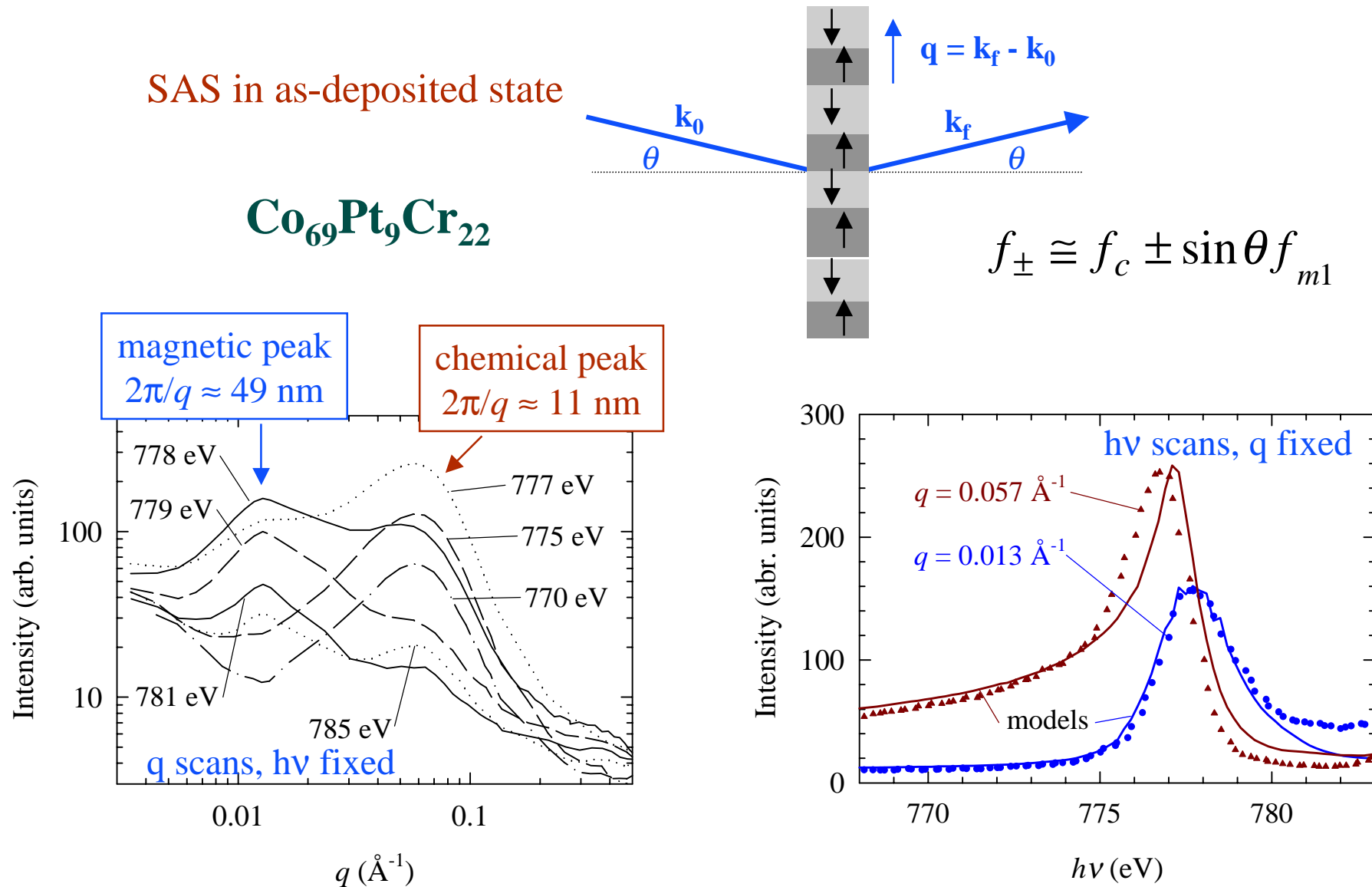
JMMM 240, 325 (2002)
APL 80, 1234 (2002)

Media layers studied:

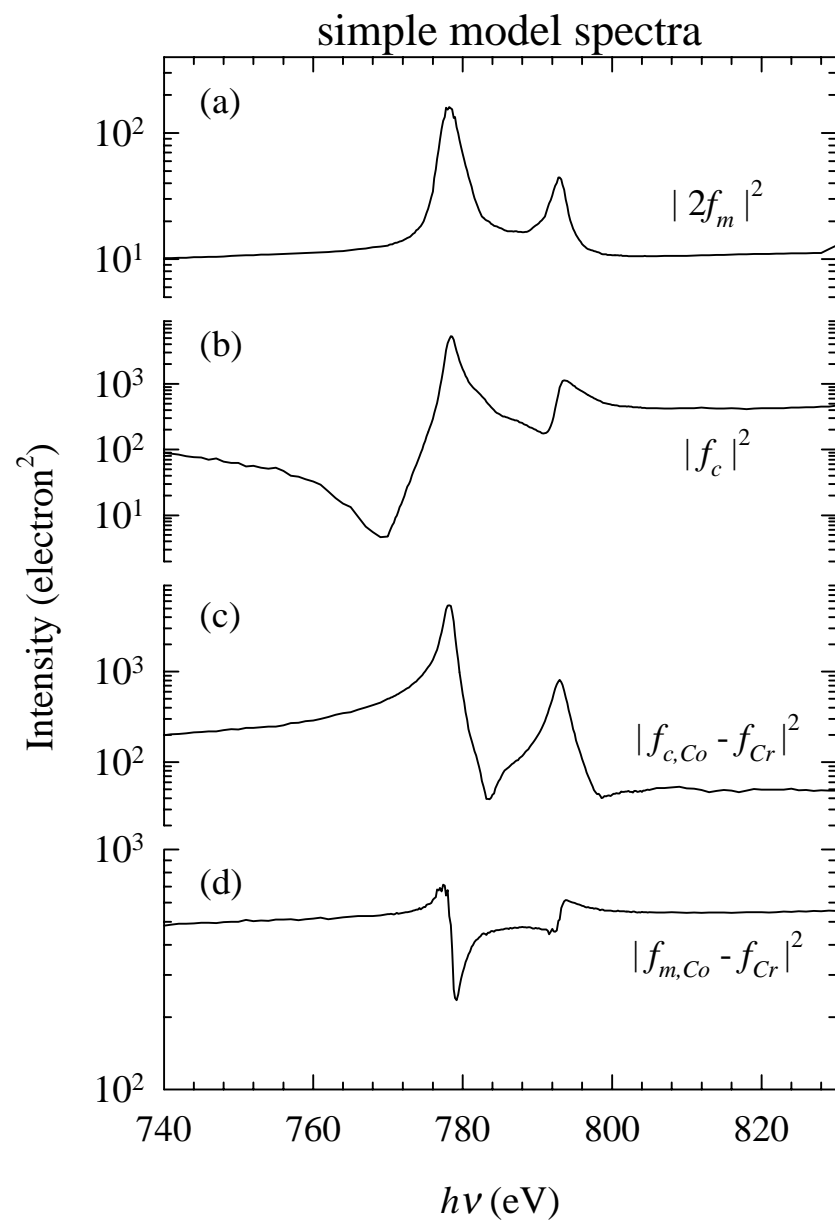
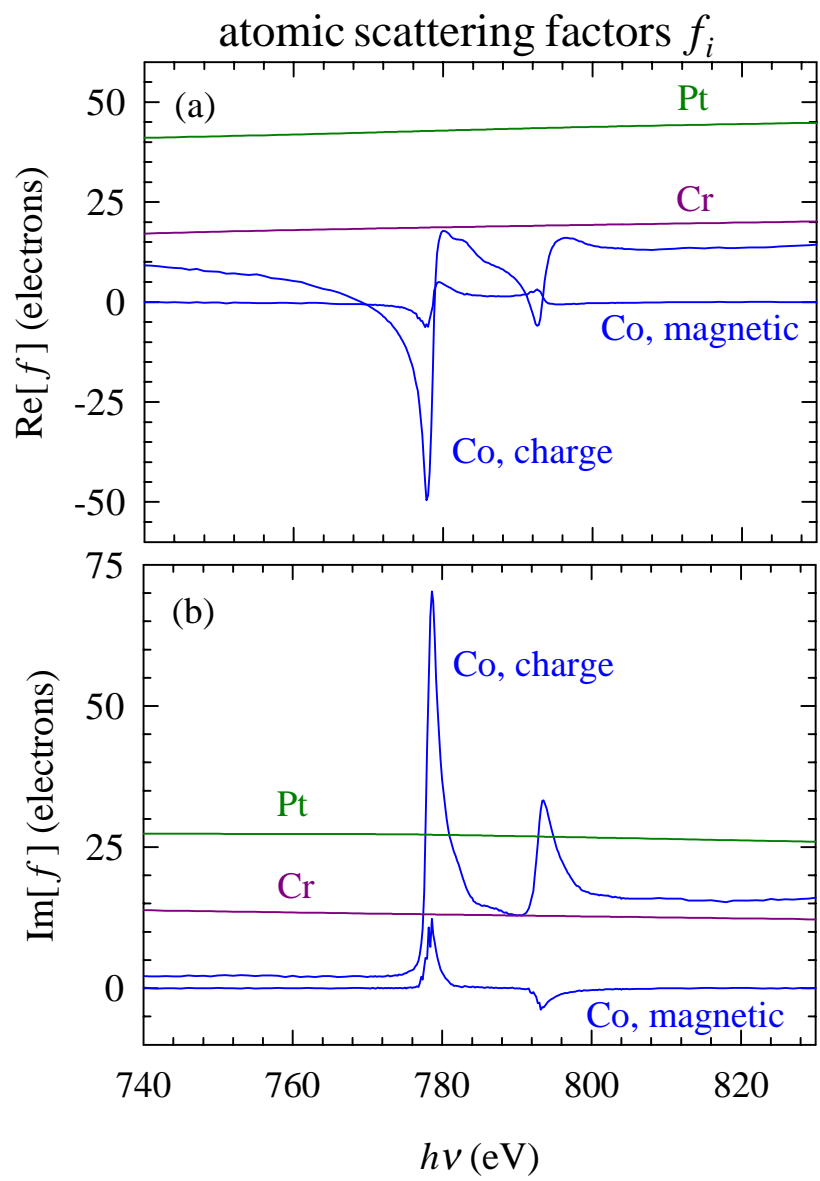
$\text{Co}_{78}\text{Cr}_{22}$
 $\text{Co}_{69}\text{Pt}_9\text{Cr}_{22}$
CoPtCrB (35 Gbit/in²)



SAS from CoPtCr: two distinct peaks, magnetic & chemical.

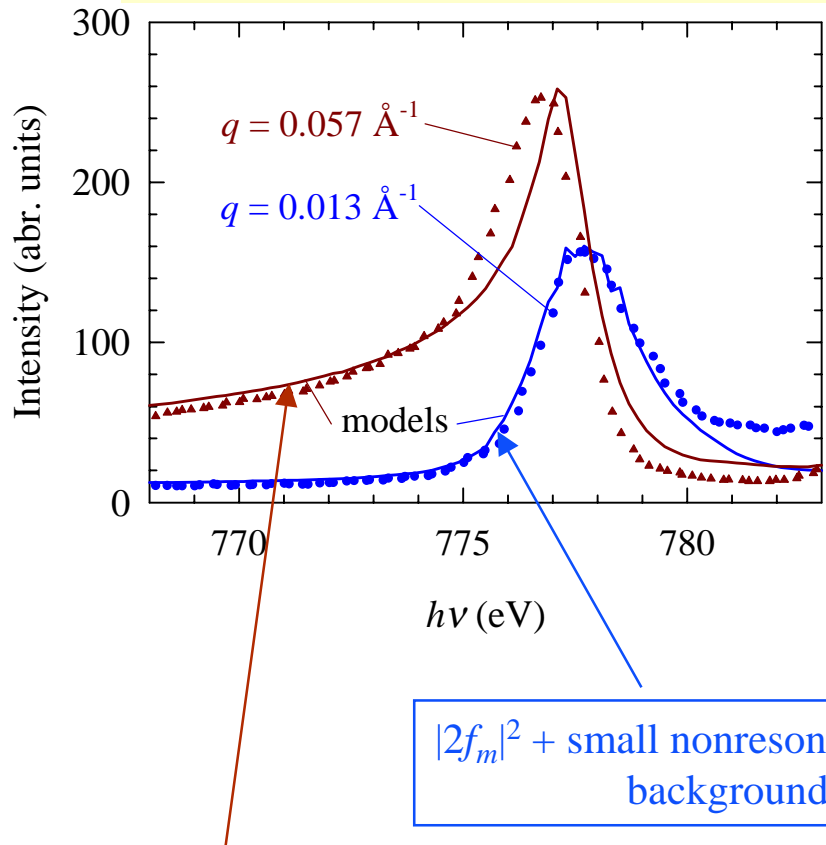


Modeling Co SAS spectra uses measured Co, tabulated Cr, Pt scattering factors.

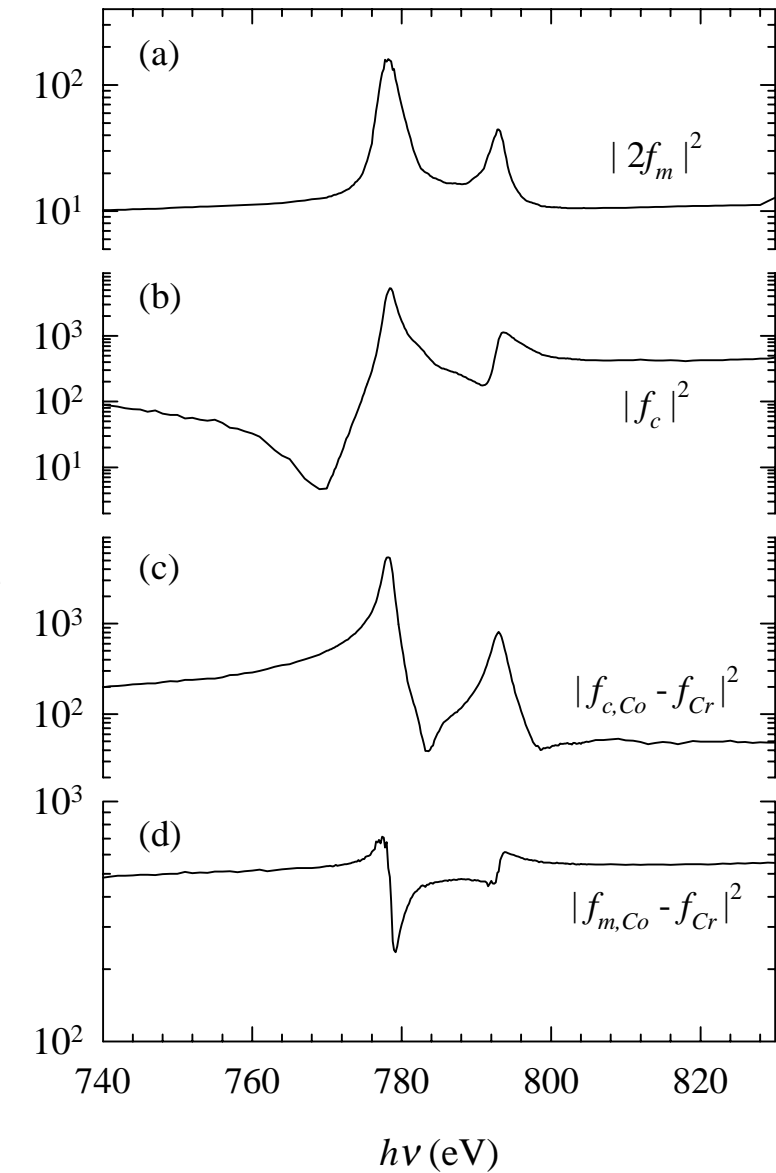


Spectral modeling sensitive to chemical composition.

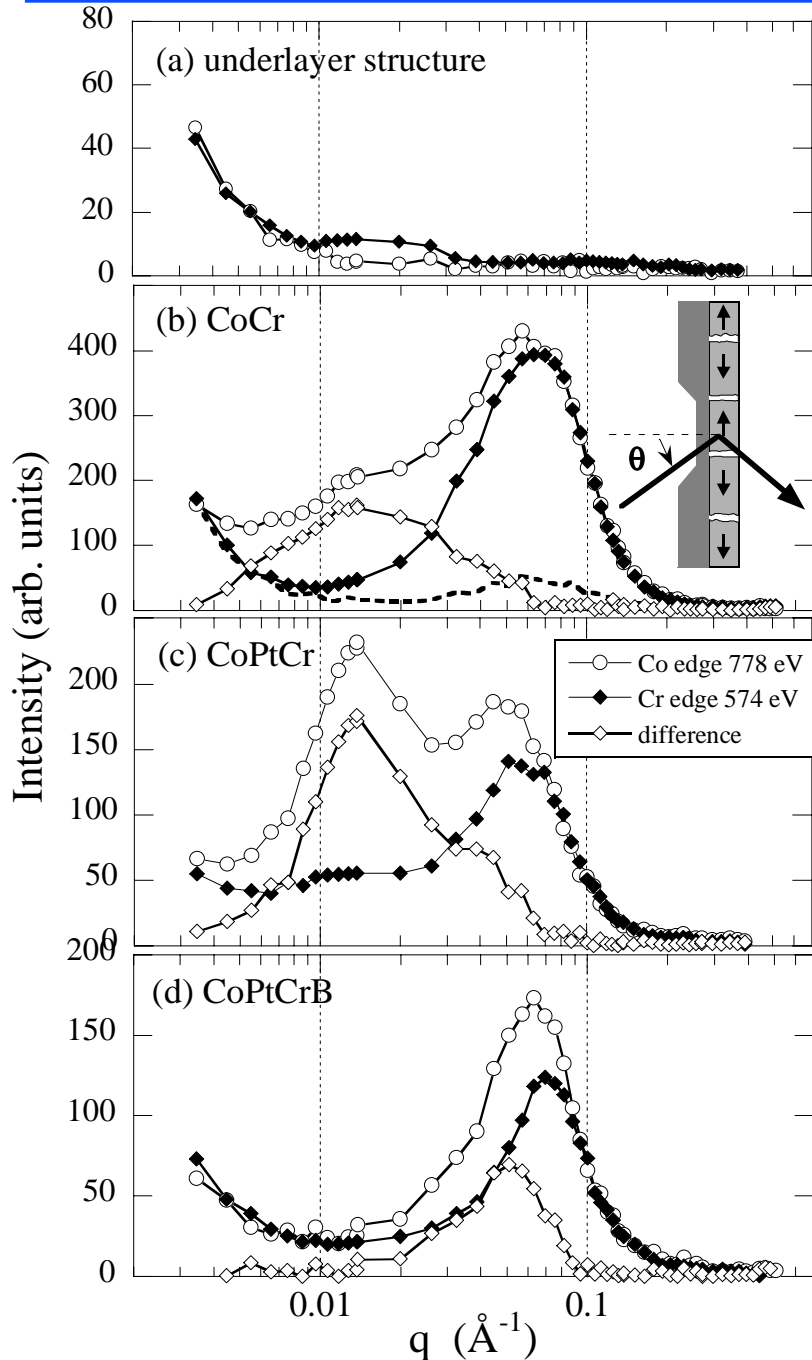
$$I = (A^* A) T, \quad A = a_1 - a_2, \quad a \propto \sum_i x_i f_i$$



Pure chemical scattering between two phases:
 $A = (20f_{c,Co} + 2f_{Pt} + f_{Cr}) - (f_{c,Co} + f_{Cr})$



Effects of added boron clearly seen in resonant SAS.



Assume:

- Co SAS shows magnetic *and* chemical correlations
- Cr SAS shows predominantly chemical correlations.

Then, their difference reveals magnetic correlations.

Sample	Grain size (\AA)	Mag. correlation length (\AA)
CoCr	95	420
CoPtCr	105	450
CoPtCrB	88	~120

Adding boron:

- Shortens magnetic correlations (close to chemical correlations), by reducing magnetic exchange coupling between grains *and* by decoupling magnetic grains from substrate.
- Little effect on chemical grain size.
- Sharpens both chemical & magnetic distributions.

Summary

Resonant MO effects provide many opportunities to resolve magnetic and chemical structure and behavior at relevant length scales in a broad range of materials.

XMOKE laterally averages but can depth resolve in various ways.

Scattering can probe in-plane structure with resolution ~ 1 nm.

Knowledge of complete MO constants necessary to fully exploit these techniques.

Useful soft x-ray resonant scattering effects are not limited to magnetic systems.